the chin appears deeper than the neck; the convexity of the face becomes concave; nose points inwards. Latency can be reduced by concentrating the gaze on the tip of the nose in the fused image. Masking of the texture of the skin is evident, but most facial features can be recognized without difficulty (Fig. 4). In this stereogram familiarity with the object is clearly a very prominent feature; yet familiarity does not prevent reversal. In contrast, when texture perspective is natural (Fig. 6), the fused image defies any effort to the perceived as inverted.

The creation of a neutral texture perspective has the effect in a monocular view of introducing some flatness into the impression of the face, much as if it had been painted on coarse canvas. Most textures with a sufficiently high density and an approximately uniform distribution of elements proved effective in neutralizing texture perspective. All concave or convex objects (for example, balls, bowls, and boxes) we investigated could be reversed in depth, regardless of familiarity or complexity of shape.

Our stereogram confirms Julesz' emphasis on the role of global factors in binocular depth perception. Neutralizing texture perspective has the binocular effect of eliminating texture perspective disparity. In this way texture perspective is made ineffective as a global binocular depth cue, while the disparity of other global image features, like clusters of texture elements, remains compatible with the disparity of local texture elements. The failure of pseudoscopy when texture perspective disparity is present, shows that a cooperation between local and global disparity information is essential for binocular depth perception.

REFERENCES AND NOTES

1. C. Wheatstone, *Philos. Mag.* **4**, 504 (1852).
2. B. Julesz, *Foundations of Cyclopean Perception* (Univ. of Chicago Press, Chicago, IL, 1971).
3. M. A. Georgeson, *Percept.* **8**, 585 (1979).
4. Readers not being in the possession of a stereoscope or prism can try to fuse the stereogram by crossing their eyes. This can be done by slowly moving a pencil or finger from the stereogram toward the eyes, while concentrating the gaze on the tip. In this way the images should shift until three images are apparent; the middle image will come to depth; the outer images should be disregarded. For a first attempt the reader is advised to fuse the line stereogram: a downward pointing pyramid indicating correct pseudoscopic fusion. Fused images may initially look unsharp, but after a few seconds the eyes will accommodate. We found fusion and accommodation relatively easy with the stereogram held at arm's length.
5. Anaglyphs are constructed by superimposing the left and right views of a stereogram in red and green. To appreciate the depth effect the anaglyphs have to be viewed through a red-green stereo viewer, which separates the original images by filtering, based on the physical wavelengths of light: the eye with the red filter in front can only see the green image and the eye with the green filter in front sees only the red image. The image in depth may not instantly be apparent, since the eyes have to adapt to the filters and to the disparity in the fused image. Good color vision is not necessary, but viewing in good light is essential. Some residual images cannot be avoided, particularly when anaglyphs are reproduced by a regular four-color printing process. For this reason we developed a yellow-green background, which masks most of the red and green residues.

6. We are grateful to R. M. Steinman for critical reading of the manuscript and to J. Brinkman and W. Rÿnders of the Amsterdam School of Graphics for preparing the anaglyphs.

5 July 1988; accepted 28 October 1988

Crystal Versus Solution Structures of Enzymes: NMR Spectroscopy of a Crystalline Serine Protease

STEVEN O. SMITH,* SHAUNA FARR-JONES, ROBERT G. GRIFFIN, WILLIAM W. BACHOVCHIN†

The hydrogen-bonding status of His^{57} in the catalytic triad (Asp-His-Ser) of serine proteases has important mechanistic implications for this class of enzymes. Recent nitrogen-15 nuclear magnetic resonance (NMR) studies of α-lytic protease find His^{57} and Ser^{195} to be strongly hydrogen-bonded, a result that conflicts with the corresponding crystallographic studies, thereby suggesting that the crystal and solution structures may differ. This discrepancy is addressed and resolved in a nitrogen-15 NMR study of the enzyme in the crystalline state. The results show that the His-Ser and Asp-His interactions are identical in crystals and solutions, but that in crystals His^{57} titrates with a pK_a of 7.9, nearly one pK_a unit higher than in solution. This elevated pK_a accounts for the absence of the His-Ser hydrogen bond in previous x-ray studies.

MOST HIGH-RESOLUTION STRUCTURAL information about proteins comes from x-ray diffraction studies of crystals, whereas functional properties of proteins are usually studied in solution. Thus, the question of whether or not the crystal and solution structures are the same often arises when functional properties are correlated with structure. In the case of enzymes, this question can be especially troublesome, because even small differences in the positions of key functional groups can have important mechanistic implications, and such differences have frequently been noted.

A case in point is the apparent discrepancy concerning the hydrogen-bonding status between His^{57} and Ser^{195} in the active site of serine proteases. Recent solution NMR studies (*1*) of α-lytic protease (α-LP, E.C. 3.4.21.12) have provided evidence for a His-Ser hydrogen bond based on the ^{15}N chemical shifts of the active site His. However, these results conflict with the x-ray crystallographic studies of α-LP (*2–4*) [and of other serine proteases (*5–9*)], which have concluded that Oγ of Ser^{195} and Nε2 of His^{57} are too far apart and not properly aligned to form a hydrogen bond. This discrepancy, though small, nevertheless has important implications for the catalytic mechanism of these enzymes, a mechanism that has been the subject of intense interest and debate (*10–13*). To summarize, the existence of this hydrogen bond would indicate a role for the Asp-His diad in activating the serine hydroxyl group for nucleophilic attack on the substrate. In its absence, such activation would probably not take place, instead the Asp-His diad may be more important in catalyzing the breakdown of the tetrahedral intermediate.

The above discrepancy between the solution and crystalline state studies does not prove that the solution and crystal structures of the enzyme are different. Instead, it raises the question of whether or not either the NMR or x-ray diffraction data could have been misinterpreted or in some other way be in error. (This would be true of any such comparison involving the results of different techniques.) To address this question, we have carried out a ^{15}N NMR study of α-LP in the crystalline state using magic angle spinning (MAS). The results provide a direct comparison with the corresponding solution state study, thereby eliminating the uncertainty described above associated with comparing interpretations of nonequivalent experimental data.

The solution ^{15}N NMR work (*1*), which

S. O. Smith and R. G. Griffin, Francis Bitter National Magnet Laboratory, Massachusetts Institute of Technology, Cambridge, MA 02139.
S. Farr-Jones and W. W. Bachovchin, Department of Biochemistry, Tufts University, School of Medicine, Boston, MA 02111.

*Present address: Department of Molecular Biophysics and Biochemistry, Yale University, New Haven, CT 06511.
†To whom correspondence should be addressed.

provided the evidence for the existence of a strong His-Ser hydrogen bond, also confirmed the presence of the Asp-His hydrogen bond, both at high (His[57] neutral) and low (His[57] protonated) *p*H and presented a framework for interpreting the ^{15}N chemical shift behavior of histidyl residues. The ring nitrogens of His can exist in three different bonding states as listed in Table 1 where NH and =N- refer to the protonated and nonprotonated nitrogens, respectively, within a neutral imidazole ring, whereas +NH refers to both nitrogens within a protonated imidazole ring. Hydrogen bonding typically induces an 8- to 10-ppm change in chemical shift of these nitrogens, moving the hydrogen bond donor NH and +NH types of nitrogen downfield while moving the hydrogen bond acceptor nitrogen (=N- type) upfield.

For α-LP in solution at *p*H 4.0, where His[57] is fully protonated (pK_a ~7.0), Nδ1 and Nε2 resonate at 191.6 and 204.2 ppm, respectively. The low-field position of Nδ1, ~10 ppm downfield from that of +NH nitrogens, reveals the presence of the hydrogen bond to Asp[102]. At *p*H 9.5, where His[57] is fully neutral, Nδ1 and Nε2 resonate at 199.4 and 138 ppm, respectively. Specific sulfonylation with phenylmethylsulfonyl fluoride (PMSF) or phosphorylation with DFP of Ser[195] induces Nε2 to move ~10 ppm downfield to ~128 while Nδ1 remains at ~200 ppm, and thus provides compelling evidence for a strong His-Ser hydrogen bond in solution. [See (*1*) for a detailed discussion of these results.]

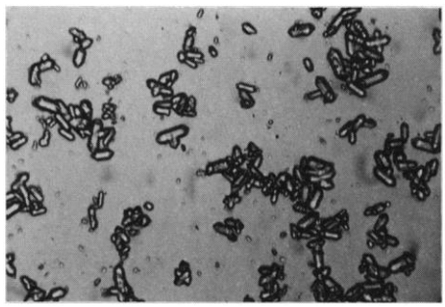

Fig. 1. Crystals of ^{15}N-labeled α-LP used for solid-state NMR. α-LP was crystallized from 0.6*M* Li_2SO_4, *p*H 5.7, 20 mg of enzyme per milliliter. [^{15}N]His–labeled α-LP was produced by culturing a His-requiring mutant of *Lysobacter enzymogenes* (ATCC 29487) with [^{15}N]His and isolated as previously described (*22*). Enzyme seed crystals were obtained at room temperature by the hanging drop method with 1.0 to 1.3*M* Li_2SO_4, *p*H 7.0, and about 10 mg of enzyme per milliliter. Larger quantities of crystals were produced by adding the above seed crystals to solutions containing 0.6*M* Li_2SO_4, *p*H 5.7, and 20 mg of enzyme per milliliter. The crystals appeared to be identical to those used in the x-ray work (*23*).

On the basis of the solution NMR results outlined above, we expected high-resolution ^{15}N NMR spectra of crystalline enzyme, under conditions where His[57] is neutral, to yield one of two possible results, that is, Nε2 at either ~138 or ~128 ppm. The first result, Nε2 at 138 ppm, would show that crystals and solutions are the same and, therefore, that the discrepancy must arise from misinterpretation of experimental data, either x-ray or NMR. The second result, that is, Nε2 at 128 ppm, would show that the His-Ser hydrogen bond is indeed absent in crystals, thereby establishing that the solution and crystal structures are different with respect to this structural feature.

Representative ^{15}N NMR spectra (*14*) of α-LP crystals (Fig. 1) at a series of *p*H values (*15*) are shown in Fig. 2. The *p*H-independent signal at ~255 ppm arises from the amide nitrogens of the peptide backbone at natural abundance ^{15}N. At low *p*H (<7.0), where His[57] is fully protonated, Nδ1 and Nε2 resonate at 192.8 and 202.2 ppm, respectively (Fig. 2A), similar to their chemical shifts in corresponding solution-state spectra. The low-field position of Nδ1 demonstrates the presence of the Asp-His hydrogen bond. As the *p*H is increased, the Nδ1 and Nε2 resonances at 192.8 and 202.2 ppm gradually decrease in intensity, while new Nδ1 and Nε2 resonances from the neutral form of His[57] appear at 197.2 and 136.5 ppm, respectively. A neutral imidazole ring with these ^{15}N shifts shows that crystals and solution are the same with respect to His-Ser hydrogen bonding. (The lower intensity of the Nε2 resonance at 136.5 ppm compared to the 202-ppm resonance results from decreased cross-polarization (CP) efficiency of nonprotonated versus protonated nitrogens and does not reflect a population difference.) The slow exchange between the protonated and neutral forms of His[57] we observed contrasts with the fast exchange observed in the solution studies. Nevertheless, the ^{15}N chemical shifts ascribed to the protonated and neutral forms of His[57] in the solution studies are remarkably similar to those observed here for enzyme crystals.

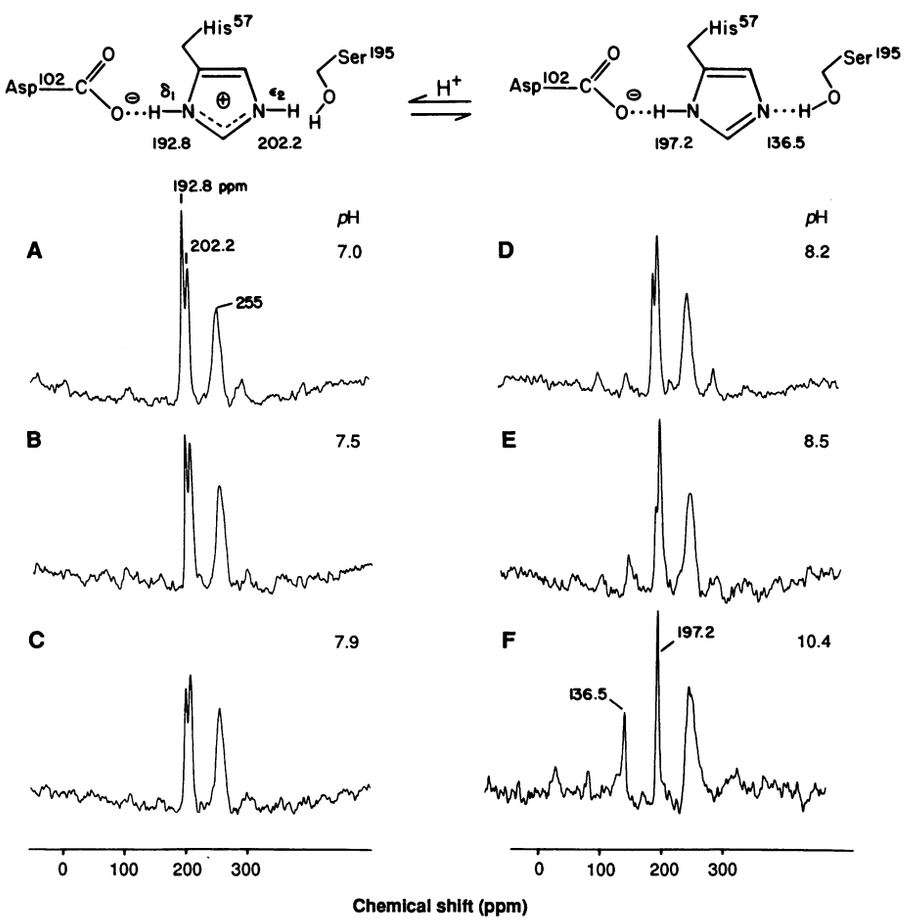

Fig. 2. CP-MAS ^{15}N NMR spectra of doubly ^{15}N-labeled α-LP crystals as a function of *p*H. The 192.8-ppm resonance moves to 197.2 ppm, whereas the 202.2-ppm resonance moves to 136.5 ppm as the *p*H is increased. The CP mixing time was 2 ms. Chemical shifts are relative to 1*M* ^{15}N-labeled $H^{15}NO_3$ referenced to the amide backbone centered at 255 ppm. Each spectrum represents 10,000 to 20,000 scans.

A potentially important difference between crystals and solutions emerges from the titration curve of His^{57} in crystals. The titration curve is most easily followed by integrating the intensity of the 192.8-ppm signal. A plot of the intensity versus *p*H (Fig. 3) indicates that His^{57} in crystals has a pK_a of ~7.9 (± SEM of 0.1) (*16*), nearly one pK_a unit higher than in solution. This result explains the discrepancy between the x-ray and NMR work on the existence of the His-Ser hydrogen bond because at the *p*H of the x-ray work (*2*), 7.2, His^{57} would be mostly protonated and thus unable to act as a hydrogen bond acceptor for the serine hydroxyl proton. Protonated His^{57} also does not form a hydrogen bond with Ser^{195} with Nε2-H acting as the donor atom in either crystals or solutions as demonstrated by the ^{15}N shifts of Nε2, which are typical for a non–hydrogen-bonded +NH type nitrogens.

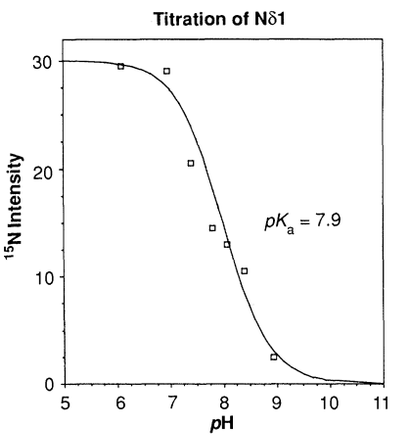

Fig. 3. Plot of Nδ1 signal intensity (relative to the intensity of the amide backbone) as a function of *p*H. The solid line is a calculated titration curve for a pK_a of 7.9.

Thus, the present work shows that the x-ray diffraction and NMR studies, although apparently in conflict, are nevertheless both correct. The discrepancy arises from the altered pK_a value of His^{57} in crystals. Why the pK_a is higher in crystals is still unclear. Preliminary results indicate that most of the $+\Delta 0.9$ pK_a change can be attributed to the high Li_2SO_4 concentrations necessary to stabilize the crystals and, moreover, that it may be a sulfate anion–specific effect as Li_2SO_4 appears to have a similar effect on the His^{57} pK_a in solutions (*17*). The low temperatures we used are unlikely to contribute significantly to the elevated pK_a as the measured pK_a of His^{57} was the same at 240 K and 170 K.

The behavior of the ^{15}N signals of His^{57} of α-LP was also examined in frozen solutions (170 K). The results show that under these conditions the protonated and neutral forms of His^{57} could also be observed and that they have ^{15}N chemical shifts similar to those observed for the solution and crystalline state enzymes (Fig. 4).

^{15}N NMR spectroscopy thus demonstrates that the overall structure of the Asp-His-Ser catalytic triad is remarkably similar in crystals and solutions. The ^{15}N chemical shifts indicate that these three residues form a strongly hydrogen-bonded system, much as originally proposed by Blow *et al.* (*18*). This structure implies that the Asp-His diad plays a role in activating the serine hydroxyl group for nucleophilic attack. Recent site-specific mutagenesis experiments in which Asp^{102} was changed to Asn in trypsin support this view because this change not only substantially disrupted catalysis, it also substantially lowered the intrinsic reactivity of Ser^{195} to reagents such as DFP (*19–21*). The later result points to a role for the Asp-His diad in activating the serine for nucleophilic attack and thus correlates with our results, which show that the Asp-His diad is strongly hydrogen-bonded to Ser^{195} in the resting enzyme.

The present study demonstrates the complementary nature of NMR spectroscopy and x-ray crystallography and the valuable role solid-state NMR can play in bridging solution and crystalline state studies.

Table 1. ^{15}N chemical shifts of imidazole nitrogens.

Nitrogen type	$^{15}N\delta$ (ppm)	$^{15}N\delta$ (ppm) in hydrogen bond
NH	210	200
=N-	128	138
+NH	201	191

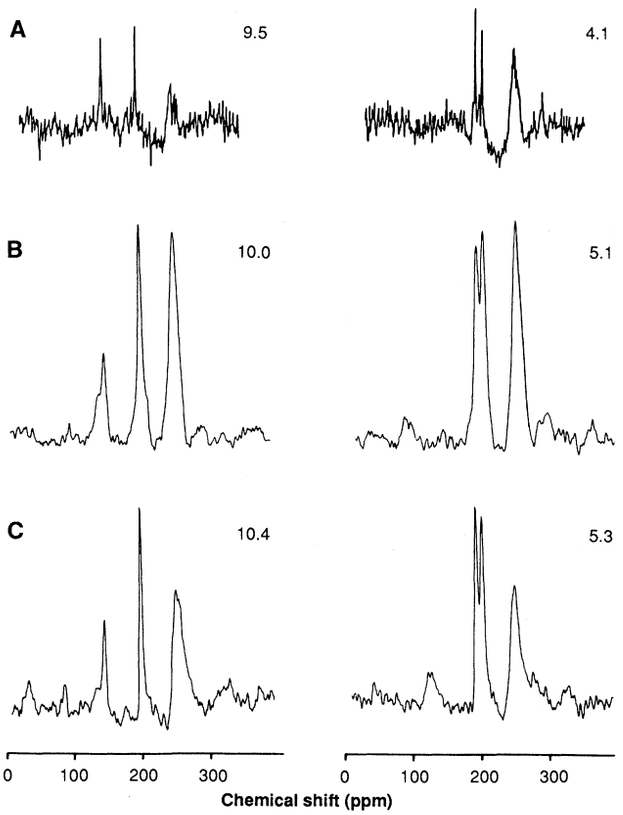

Fig. 4. Comparison of the ^{15}N NMR spectra of doubly labeled α-LP in solution (**A**), frozen solution (**B**), and in crystals (**C**). High-*p*H spectra (9.5 to 10.4) are in the left-hand column and low-*p*H spectra (4.1 to 5.3) are in the right-hand column. Spectra (B) and (C) were obtained with CP mixing times of 1.5 ms, resulting in slightly different intensities relative to those in Fig. 2.

REFERENCES AND NOTES

1. W. W. Bachovchin, *Biochemistry* **25**, 7751 (1986).
2. G. D. Brayer, L. T. J. Delbaere, M. N. G. James, *J. Mol. Biol.* **131**, 743 (1979).
3. L. T. J. Delbaere, G. D. Brayer, M. N. G. James, *Nature* **279**, 165 (1979).
4. M. Fujinaga, L. T. J. Delbaere, G. D. Brayer, M. N. G. James, *J. Mol. Biol.* **183**, 479 (1985).
5. G. H. Cohen, E. W. Silverton, B. W. Matthews, H. Braxton, D. R. Davies, *ibid.* **44**, 129 (1969).
6. W. Bode and P. Schwager, *ibid.* **98**, 693 (1975).
7. D. A. Matthews, R. A. Alden, J. J. Birktoft, S. T. Freer, J. Kraut, *J. Biol. Chem.* **252**, 8875 (1977).
8. A. R. Sielecki, W. A. Hendrikson, G. C. Broughton, L. T. J. Delbaere, G. D. Brayer, M. N. G. James, *J. Mol. Biol.* **134**, 781 (1979).
9. M. N. G. James, A. R. Sielecki, G. D. Brayer, L. T. J. Delbaere, C.-A. Bauer, *ibid.* **144**, 43 (1980).
10. J. Kraut, *Annu. Rev. Biochem.* **46**, 331 (1977).
11. J. L. Markley *et al.*, in *Frontiers in Protein Chemistry*, T.-Y. Liu, G. Mamiya, K. T. Yasunobu, Eds. (Elsevier/North-Holland, New York, 1980), pp. 31–61.
12. T. A. Steitz and R. G. Shulman, *Annu. Rev. Biophys. Bioeng.* **11**, 419 (1982).
13. R. L. Schowen, in *Mechanistic Principles of Enzyme Activity*, J. F. Liebman and A. Greenberg, Eds. (VCH, New York, 1988), pp. 119–168.
14. High-resolution solid-state ^{15}N NMR spectra of specifically [^{15}N]His^{57}-labeled α-LP in the crystalline state (Fig. 1) were obtained with MAS at ~170 K and at ~240 K with a standard cross-polarization (CP) pulse sequence. Acquisition time was 10 ms, with a recycle delay of 3 s. CP from the ^1H to ^{15}N spin systems was used to increase the ^{15}N sensitivity

and shorten the effective ^{15}N T_1. Previous solid-state NMR studies on α-LP (*24*) indicated an optimal mixing time for CP of 0.3 ms for protonated nitrogens and 2 ms for nonprotonated nitrogens. Mixing times of 1.5 to 2 ms were used for the spectra reported here. The ^{15}N and ^1H frequencies were 32 and 318 MHz, respectively, and the ^1H 90° pulse length was 3.0 μs. The sample temperature was maintained near 170 K or 240 K with cooled N_2 as the spinning gas. The low temperature served to increase sensitivity and reduce dielectric heating of the sample.

15. To adjust the *p*H of the enzyme crystals for *p*H-dependent NMR studies, the crystals were separated from the mother liquor by mild centrifugation and resuspended in 0.6*M* Li_2SO_4 at the desired *p*H and incubated at room temperature for ~15 min to allow for equilibration throughout the crystal. [The meaning of *p*H and pK_a in solid samples has been discussed (*24, 25*). The process was repeated until equilibration at the desired *p*H was attained. The *p*H of the mother liquor was measured on a Radiometer *p*H meter (model 260) with a combination electrode (model GK2322C) at 295 K. The titration was reversible, the direction of the titration did not affect the relative intensities of the NMR resonances. Also, the entire titration was repeated on the same crystals and spectra recorded at 240 K. Chemical shifts are relative to external 1*M* $H^{15}NO_3$ in ^2H_2O, with positive shifts being upfield, and referenced to the *p*H independent signal of the natural abundance ^{15}N amide backbone resonance at 255 ppm. No correction was made for bulk magnetic susceptibility effects which are expected to be small.
16. Intensity of the $^{15}N\delta1$ signal as a function of *p*H was fit to the Henderson-Hasselbalch equation with the use of the program *Enzfitter—A Nonlinear Data Analysis Program for the IBM PC* [R. Leatherbarrow (Elsevier-Biosoft, Cambridge, 1987)].
17. Solution state ^{15}N NMR studies show that the addition of 0.6*M* Li_2SO_4 to a solution of α-LP in 0.1*M* KCl increases the pK_a of His^{57} from 7.0 to 7.5 (S. Farr-Jones and W. W. Bachovchin, unpublished data).
18. D. M. Blow, J. J. Birktoft, B. S. Hartley, *Nature* **221**, 337 (1969).
19. C. S. Craik, S. Roczniak, C. Largeman, W. J. Rutter, *Science* **237**, 909 (1987).
20. S. Sprang *et al.*, *ibid.*, p 905.
21. P. Carter and J. A. Wells, *Nature* **332**, 564 (1988).
22. W. W. Bachovchin and J. D. Roberts, *J. Am. Chem. Soc.* **100**, 8041 (1978).
23. M. N. G. James and L. B. Smillie, *Nature* **224**, 694 (1969).
24. T. H. Huang, W. W. Bachovchin, R. G. Griffin, C. M. Dobson, *Biochemistry* **23**, 5933 (1984).
25. M. Munowitz *et al.*, *J. Am. Chem. Soc.* **104**, 1192 (1982).
26. Supported by NIH research grants GM 27927 and GM 23403, a postdoctoral fellowship to S.O.S. (GM 10502), Research Career Development Award to W.W.B. (DK 01122), and NSF equipment grant PCM 8212656. The Stable Isotopes Resource of the Los Alamos National Laboratory provided $^{15}NH_3$ for the synthesis of the ^{15}N-labeled histidines with the aid of NIH grant RR 02231. We thank D. Agard for advice on crystallizing α-LP and helpful discussions.

12 December 1988; accepted 14 March 1989

Ice Core Evidence for Extensive Melting of the Greenland Ice Sheet in the Last Interglacial

R. M. KOERNER

Evidence from ice at the bottom of ice cores from the Canadian Arctic Islands and Camp Century and Dye-3 in Greenland suggests that the Greenland ice sheet melted extensively or completely during the last interglacial period more than 100 ka (thousand years ago), in contrast to earlier interpretations. The presence of dirt particles in the basal ice has previously been thought to indicate that the base of the ice sheets had melted and that the evidence for the time of original growth of these ice masses had been destroyed. However, the particles most likely blew onto the ice when the dimensions of the ice caps and ice sheets were much smaller. Ice texture, gas content, and other evidence also suggest that the basal ice at each drill site is superimposed ice, a type of ice typical of the early growth stages of an ice cap or ice sheet. If the present-day ice masses began their growth during the last interglacial, the ice sheet from the earlier (Illinoian) glacial period must have competely or largely melted during the early part of the same interglacial period. If such melting did occur, the 6-meter higher-than-present sea level during the Sangamon cannot be attributed to disintegration of the West Antarctic ice sheet, as has been suggested.

INTERPRETATION OF THE AGE AND mode of origin of the ice sheets and ice caps has been difficult because drag and melting at the base of these ice sheets may have disturbed or removed the record in the deepest and oldest ice. Studies of oxygen isotopes ($\delta^{18}O$) and pollen concentrations in a core from the top of the flow line on Agassiz ice cap, Ellesmere Island, Canada (Fig. 1), led to the conclusion that the lowermost 3 m of ice were deposited during the last (Sangamon) interglacial period (*1*). The location must, therefore, have been ice-free earlier during the same interglacial. Because of certain similarities among this core and others drilled from the same ice cap and on Devon ice cap, this interpretation was extended to include the Canadian Arctic Island (CAI) ice caps in general (Fig. 1) (*1*). A similar origin for the basal ice in the ice cores from Camp Century (CC) and Dye-3 (D3) (Fig. 1) has been cursorily suggested (*2, 3*), and a study of diatoms in the basal debris of the CC core showed that this drill site was ice-free during some interglacial in the past (*4*). In this report, I review the record from the Greenland and Antarctic cores to evaluate the possibility that the ice-free period at the CC and D3 drill sites was the last interglacial (*5*).

Terrain Sciences Division, Geological Survey of Canada, Ottawa, Ontario K1A OE8.

I use Core 79 from Agassiz ice cap (Fig. 2) as representative of all the CAI cores (Table 1) because it is from a drill site close to the top of the flow line and has been intensively studied (*1, 6–8*). Byrd and Vostok cores are from Antarctica; D3 and CC are located on the Greenland ice cap. Dating for all these cores has been achieved by various methods (*9–11*) but is largely speculative beyond 13 ka (*2, 12*). However, for assessing the age of the basal ice with respect to the last interglacial, a rough time scale is adequate.

There are three main sections in the $\delta^{18}O$ record of the CAI and Greenland cores (Fig. 1): (i) an uppermost one (A in Fig. 1) representing the present interglacial period (0 to 10 ka); (ii) a middle section (B) with more negative values representing the last glaciation (10 to 110 ka); and (iii) a lowermost section (C), where $\delta^{18}O$ values are less negative again. In general, negative $\delta^{18}O$ values represent cold climatic conditions and less negative values, warmer conditions. The $\delta^{18}O$ records, together with ice texture and cation, pollen, and microparticle concentrations (*1, 9, 13, 14*), indicate that the CAI cores include these three ice core sections even though the CAI ice caps are much thinner than the ice sheets of Greenland and Antarctica (Table I). The Vostok core, which does not reach bedrock, includes all these sections, spans the entire last interglacial period, and includes also part of the glacial period before that (*3*). The Byrd core covers the top two sections (*11*) and has been arguably considered to include Sangamon ice at its base (*15*).

Comparisons between the observed $\delta^{18}O$ values of the basal and mean Holocene ice in the CAI and Greenland ice cores suggest that the basal ice in all these cores was deposited during an interglacial climate (Table 2). However, correction of the Greenland ice core data is necessary to account for the effect of elevation on the basal $\delta^{18}O$ values (*17, 18*): because of the nature of glacier flow, the deepest ice forms from snow deposited on the surface well up the flow line, and $\delta^{18}O$ values become more negative with increasing elevation in Greenland (*16*). Correction of the CAI data is not necessary as, at present, elevation is not related to $\delta^{18}O$ values in the Canadian Arctic Islands (*19*), and the cores I am considering